# Characterization of cyclic and linear $C_3H^-$ and $C_3H$ via anion photoelectron spectroscopy

Sean M. Sheehan, Bradley F. Parsons,[a] Jia Zhou, Etienne Garand, Terry A. Yen, David T. Moore,[b] and Daniel M. Neumark[c]
*Department of Chemistry, University of California, Berkeley, California 94720-1460, USA and Chemical Sciences Division, Lawrence Berkeley National Laboratory, Berkeley, California 94720, USA*

(Received 6 September 2007; accepted 22 October 2007; published online 15 January 2008)

Anion photoelectron spectroscopy of $C_3H^-$ and $C_3D^-$ is performed using both field-free time-of-flight and slow electron velocity-map imaging. We observe and assign transitions originating from linear/bent ($l$-$C_3H$) and cyclic ($c$-$C_3H$) anionic isomers to the corresponding neutral ground states and low-lying excited states. Transitions within the cyclic and linear manifolds are distinguished by their photoelectron angular distributions and their intensity dependence on the neutral precursor. Using calculated values for the energetics of the neutral isomers [Ochsenfeld *et al.*, J. Chem. Phys. **106**, 4141 (1997)], which predict $c$-$C_3H$ to lie 74 meV lower than $l$-$C_3H$, the experimental results establish $c$-$C_3H^-$ as the anionic ground state and place it 229 meV below $l$-$C_3H^-$. Electron affinities of $1.999 \pm 0.003$ and $1.997 \pm 0.005$ eV are determined for $C_3H$ and $C_3D$ from the $\tilde{X}\,^2B_2 \leftarrow \tilde{X}\,^1A_1$ photodetachment transition of $c$-$C_3H$. Term energies for several low-lying states of $c$-$C_3H$ and $l$-$C_3H$ are also determined. Franck-Condon simulations are used to make vibrational assignments for the bands involving $c$-$C_3H$. Simulations of the $l$-$C_3H$ bands were more complicated owing to large amplitude bending motion and, in the case of the neutral $\tilde{A}\,^2\Pi$ state, strong Renner-Teller coupling. © *2008 American Institute of Physics*. [DOI: 10.1063/1.2812561]

## I. INTRODUCTION

The $C_3H$ radical is an important reaction product in the prototypical reaction implicated in the growth of carbon chains in interstellar clouds and circumstellar envelopes, $C(^3P) + C_2H_2 \rightarrow C_3H + H$.[1,2] Two isomeric forms of $C_3H$ have been identified in the interstellar medium, a linear/bent form ($l$-$C_3H$) and a cyclic form ($c$-$C_3H$). $l$-$C_3H$ was first produced and studied by microwave spectroscopy in the laboratory in 1985,[3] and subsequently identified in space that same year.[4] Similarly, $c$-$C_3H$ was also formed in the laboratory and found in space in 1987.[5] Following these discoveries, larger carbon-chain monohydride radicals up to $C_8H$ have been identified in carbon-rich clouds,[6] showing abundances that drop off significantly with chain length.[7] In addition, large differences in number densities between the monohydrides with odd and even numbers of carbon atom have been observed, with the even numbered chains being more abundant.[8,9] In order to model the observed number densities of interstellar molecules, it has been proposed that atom-neutral reactions be included in addition to the ion-molecule reactions traditionally thought to dominate interstellar molecular production.[1,10] Despite the relatively cold environment of interstellar space (10–50 K), atom-neutral reactions may be more important than previously thought and may even occur preferentially at lower temperatures.[2] The relevance of $C_3H$ to carbon-chain formation has motivated the work presented here, in which we investigate both structures via photoelectron spectroscopy of the $C_3H^-$ anion, finding in the process that the anion also has two structures.

The $C_3H$ radical is a very complex species for a relatively small molecule. There has been considerable theoretical and experimental effort devoted to the determination of the relative energetics and symmetry of its cyclic and linear/bent forms. Aoki *et al.*[11] calculated the two lowest energy states for both $c$-$C_3H$ and $l$-$C_3H$, with one state in each case being a slightly distorted $C_s$ structure and the other being the higher symmetry form, $C_{2v}$ and $C_{\infty v}$, respectively. Depending on the level of theory used, the energetic ordering of the higher symmetry states in relation to the $C_s$ states is reversed. In order to address this problem, Stanton[12] performed higher level calculations on the $^2B_2$ ground state of $c$-$C_3H$ and found that a pseudo-Jahn-Teller interaction with the nearby $^2A_1$ state is not strong enough to distort the equilibrium geometry from $C_{2v}$ symmetry. The $l$-$C_3H$ case is analogous to HCCO and HCCS in that the $C_{\infty v}$ structure corresponds to $a\,^2\Pi$ state, which can undergo a Renner-Teller interaction.[13] The combined effects of Renner-Teller and spin-orbit coupling in $C_3H$ were studied by Perić *et al.*[14]

In addition to the difficulties in determining the ground state symmetries of the linear/bent and cyclic isomers, their relative energies are also found to depend on the level of theory and basis set employed. Takahashi and Yamashita[15] found the bent isomer to be 22 meV more stable than the cyclic isomer at the complete active space self-consistent field (CASSCF) level of theory, but the cyclic isomer became

[a]Permanent address: Department of Chemistry, Creighton University, Omaha, NE 68178.
[b]Permanent address: Department of Chemistry, Lehigh University, Bethlehem, PA 18015.
[c]Author to whom correspondence should be addressed. Electronic mail: dneumark@berkeley.edu.

 

more stable by 68 meV using MRCI+Q. Ochsenfeld *et al.*[16] predicted the cyclic $C_{2v}$ structure to be the global minimum by about 135 meV at the CCSD(T)/cc-pVQZ level of theory with the linear $C_{\infty v}$ and bent $C_s$ forms nearly isoenergetic, a result consistent with recent work by Wang *et al.*[17] at a similar level of theory. Sancho-Garciá and Pérez-Jiménez[18] performed a basis set study at the CCSD(T) level of theory. They found that their results were not converged with respect to the largest basis set used and extrapolated to give the cyclic $^2B_2$ state as the lowest energy isomer by 144 meV. By most accounts, it appears that the cyclic isomer of neutral $C_3H$ is the global minimum, but only by a small amount.

On the experimental side, Jiang *et al.*[19] determined three frequencies of $l$-$C_3H$ using Fourier transform infrared spectroscopy in an argon matrix. Ding *et al.*[20] probed three excited states of $l$-$C_3H$, $\tilde{A}\,^2A'$, $\tilde{B}\,^2A''$, and $\tilde{C}\,^2A''$, using resonant two-photon ionization spectroscopy to excite transitions from the $^2\Pi$ ground state. For both $c$-$C_3H$ and $l$-$C_3H$, as well as $c$-$C_3D$ and $l$-$C_3D$, microwave studies performed since their discoveries have refined the determination of their lowest energy equilibrium geometries.[21–24] In the case of both isomers, it was found that they behaved spectroscopically like the higher symmetry species, although the possibility of $C_s$ equilibrium geometries was not ruled out.

There have been several theoretical calculations[25–28] and experimental studies[29–31] on the $C_3H^-$ anion. Aoki *et al.*[25] found four singlet and two triplet states of the anion, with the $^1A_1$ ($C_{2v}$) cyclic state as the global minimum. The bent $^3A''$ state was 303 meV higher in energy with the next lowest $^1A'$ state only 4 meV above the triplet. Ikuta[26] performed calculations on both $l$-$C_3H$ and $c$-$C_3H$ in order to compare relative energies, although the linear form was constrained to $C_{\infty v}$ symmetry. At the MRCI/Q level of theory, he found the cyclic form to be more stable than the linear by 310 meV. More recently Lakin *et al.*[27] calculated the anion singlet potential energy surface and found the cyclic $^1A_1$ state to be more stable than the linear $^1A'$ state by about 0.56 eV Woon[28] also found a singlet and a triplet state of the $l$-$C_3H$ anion using CCSD(T) methods and put the triplet state only 60 meV higher in energy.

The first experimental work on $C_3H^-$ was performed in 1985 by Oakes and Ellison,[31] who measured its photoelectron spectrum. They observed what appeared to be a single vibrational progression and attributed the entire spectrum to photodetachment from $l$-$C_3H^-$, although they did not definitively assign any vibrational frequencies. A more recent, lower resolution photoelectron spectrum by Kohno *et al.*[32] gave an electron affinity (EA) of 1.963 eV, although it is not clear whether this value corresponds to the linear or cyclic form.

Photodetachment and electronic spectroscopy of the anion have also been studied by[29,30] Pachkov *et al.*[29] observed resonant two-photon detachment spectra assigned to the $\tilde{b}\,^3A''\leftarrow\tilde{a}\,^3A''$ transition of $l$-$C_3H^-$ and $C_3D^-$, while Pino *et al.*[30] obtained one-photon spectra of the $\tilde{d}\,^3A''\leftarrow\tilde{a}\,^3A''$ transition in $l$-$C_3H^-$ and $C_3D^-$. In both studies, progressions in the HCC bending modes were observed and the potentials in both the upper and lower states were fitted using experimental parameters. Note that this spectroscopic notation assumes that $l$-$C_3H^-$ lies above $c$-$C_3H^-$, consistent with the theoretical work discussed above.

If, indeed, the ground state of the anion is cyclic, then it should be possible to observe and characterize this isomer spectroscopically. In this paper, we present anion photoelectron spectra and higher resolution slow electron velocity-map imaging spectra of $C_3H^-$ and $C_3D^-$ at various photodetachment wavelengths between 658 nm (1.884 eV) and 266 nm (4.661 eV). We use different precursors to generate the anions in order to distinguish the contributions from $c$-$C_3H$ and $l$-$C_3H$ and find evidence for photodetachment from both anion isomers to the ground and excited states of both neutral isomers. In the next section, we give the details of our experiments using field-free and velocity-map imaging electron collection techniques. Section III gives the results of our experiments and electronic structure calculations. Section IV provides assignments of our spectra using previous experimental data, calculations, and Franck-Condon (FC) simulations.

## II. EXPERIMENTAL

Photoelectron spectra of $C_3H^-$ and $C_3D^-$ were taken using two anion photodetachment instruments involving different electron detection techniques. The first apparatus employed a fixed frequency laser to detach electrons, which were then collected with a field-free time-of-flight (TOF) detector.[33,34] In the second spectrometer, electrons were detached near threshold with a tunable laser and detected using slow electron velocity-map imaging (SEVI).[35] The TOF instrument yields spectra over large electron kinetic energy ranges with an energy resolution of 8–10 meV, while SEVI yields a resolution as high as 1–2 $cm^{-1}$ over narrower energy ranges.

In the TOF photoelectron spectrometer, $C_3H^-$ was formed by expanding either acetylene ($HC{\equiv}CH$) or propyne ($H_3C{-}C{\equiv}CH$) seeded in $N_2$ through a pulsed piezoelectric nozzle followed by a high voltage discharge. The acetylene mixture consisted of 8% acetylene and 1% $CO_2$ in a balance of $N_2$, which was discharged at approximately 800 V. The propyne mixture was 3% propyne in $N_2$ discharged at 900 V. The gas pulse expanded supersonically from the discharge nozzle and was collimated by a skimmer. A Wiley-McLaren mass spectrometer extracted anions into a linear reflectron TOF mass spectrometer with a mass resolution ($m/\Delta m$) of 2000.[36] Various ion optics steered the ion packet toward the interaction region where it was intersected by the detachment laser. Detached electrons were detected using a chevron-mounted dual microchannel plate (MCP) detector at the end of a ~1 m long, magnetically shielded flight tube perpendicular to both the molecular and laser beam axes. A typical spectrum was collected over 120 000 laser shots.

For this experiment, the third (355 nm, 3.495 eV) and fourth (266 nm, 4.661 eV) harmonics of a Nd:YAG (yttrium aluminum garnet) laser were used. The laser polarization angle ($\theta$), the angle between the electric field vector of the laser and the direction of electron collection, was set to either

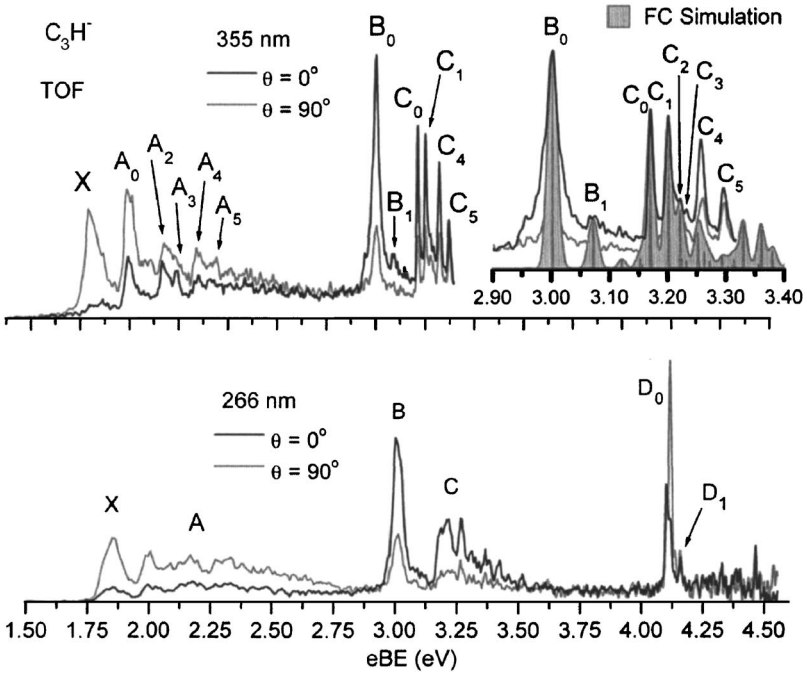


FIG. 1. TOF photoelectron spectra of $C_3H^-$ using propyne precursor at 355 nm (top) and 266 nm (bottom) plotted in electron binding energy (eBE). Black and gray traces are taken at laser polarization angles of 0° and 90°, respectively. The inset in the top panel shows an expanded view of bands *B* and *C* between 2.9 and 3.4 eV along with their Franck-Condon (FC) simulation.

0° or 90° in order to obtain angular information of the photoelectrons. The angular distribution of the photoelectrons is given by[37]

$$\frac{d\sigma}{d\Omega} = \frac{\sigma_{\text{total}}}{4\pi}\left[1 + \frac{\beta}{2}(3\cos^2\theta - 1)\right], \quad (1)$$

where $\theta$ the laser polarization angle, $\sigma_{\text{total}}$ is the total photodetachment cross section, and $\beta$ is the anisotropy parameter which varies from −1 to 2. Each feature in the photoemission spectrum has a characteristic $\beta$ calculated using the equation

$$\beta = \frac{I_{0^\circ} - I_{90^\circ}}{1/2I_{0^\circ} + I_{90^\circ}}, \quad (2)$$

where $I_{0^\circ}$ and $I_{90^\circ}$ are the intensities of the peak taken at $\theta$=0° and 90°. In the work presented here, the anisotropy parameter was found to be quite useful as a probe of vibronic coupling and as a means of distinguishing close-lying neutral←anion electronic transitions.

In the SEVI instrument, $C_3H^-$ and $C_3D^-$ anions were produced by expanding either ~1% propyne or ~1% methyl-$d_3$-acetylene ($D_3C-C\equiv CH$, C/D/N isotopes) in an approximately 50:50 mixture of $CO_2$:Ar into the source vacuum chamber through an Even-Lavie pulsed valve[38] equipped with a circular ionizer. Ions were extracted perpendicularly into a Wiley-McLaren TOF mass spectrometer ($m/\Delta m \sim 400$) and directed through a 3 mm pinhole in the repeller of a collinear velocity-map imaging (VMI) stack. The VMI stack comprised a repeller plate held at constant negative potential of either 250 or 350 V, an extractor plate held at 70% of the repeller potential, and a ground plate. A lower repeller voltage resulted in greater magnification of the images on the detector and improved resolution.[35] Electrons were detached with a Nd:YAG pumped, tunable nanosecond-dye laser in the interaction region located midway between the repeller and extractor plates. The laser was tuned and set to various wavelengths between 657.7 nm (1.885 eV) and 564.9 nm (2.195 eV), while data were collected. More peaks were seen in the spectrum as the photon energy was increased at the expense of decreased resolution for a particular feature.[35,39] Photoelectrons were mapped onto a MCP assembly coupled to a phosphor screen and electron hits were recorded using a digital camera. Each image was a sum of 12 000–35 000 laser shots. Images were symmetrized and transformed to recover a two-dimensional (2D) slice from the 2D projection via an inverse-Abel transform. Transformed images were then angularly integrated and converted to electron binding energy (eBE) for analysis. Angular information of photoelectrons was obtained directly from the transformed images through fits to Eq. (1).

## III. RESULTS

### A. Photoelectron spectra

Figure 1 shows the TOF photoelectron spectra of $C_3H^-$ at 355 nm (3.495 eV, top) and 266 nm (4.661 eV, bottom). All spectra in Fig. 1 were taken using the propyne precursor. For both wavelengths, spectra were collected at laser polarization angles of 0° (black trace) and 90° (gray trace). The spectra are plotted in eBE from 1.5 to 4.6 eV. Equal numbers of laser shots were taken at both polarizations, and eBE intensities were scaled relative to raw TOF data. No features were observed below 1.6 eV. Four bands, *X*, *A*, *B*, and *C*, are indicated in the 355 nm spectrum, while the 266 nm spectrum reveals a fifth band labeled *D*. Bands seen at the same eBE in both spectra are better resolved at 355 nm as their kinetic energy is lower. In the 355 nm spectrum, band *X* consists of a single peak at about 1.84 eV, while in band *A*, one can distinguish five peaks $A_0$ to $A_5$. Band *B* consists of an intense peak, $B_0$, at approximately 3.00 eV with a smaller feature, $B_1$, at higher eBE. Band *C* is labeled as a series of

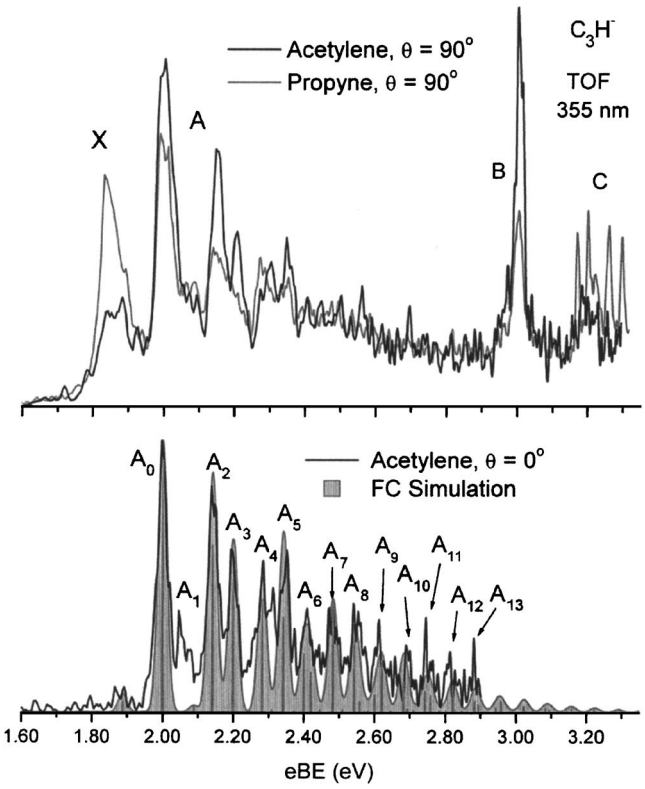


FIG. 2. Comparison of the 355 nm, $\theta$=90° TOF photoelectron spectra of $C_3H^-$ taken using acetylene (black) and propyne (gray) as precursors (top) and a portion of the 355 nm, $\theta$=0° TOF photoelectron spectrum using acetylene along with the FC simulation of the band *A* (bottom). The $\theta$=0° acetylene spectrum shows much better resolution of the *A* band into $A_0$–$A_{13}$.

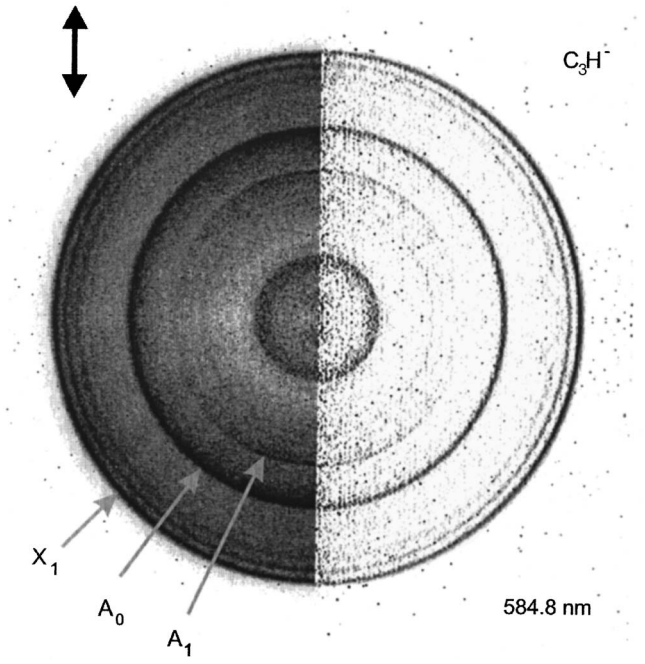


FIG. 3. SEVI photoelectron image of $C_3H^-$ at 584.8 nm (2.120 eV). The image shows the raw symmetrized (left half) and Abel transformed (right half) data. The black arrow indicates the direction of polarization of the electric field of the laser.

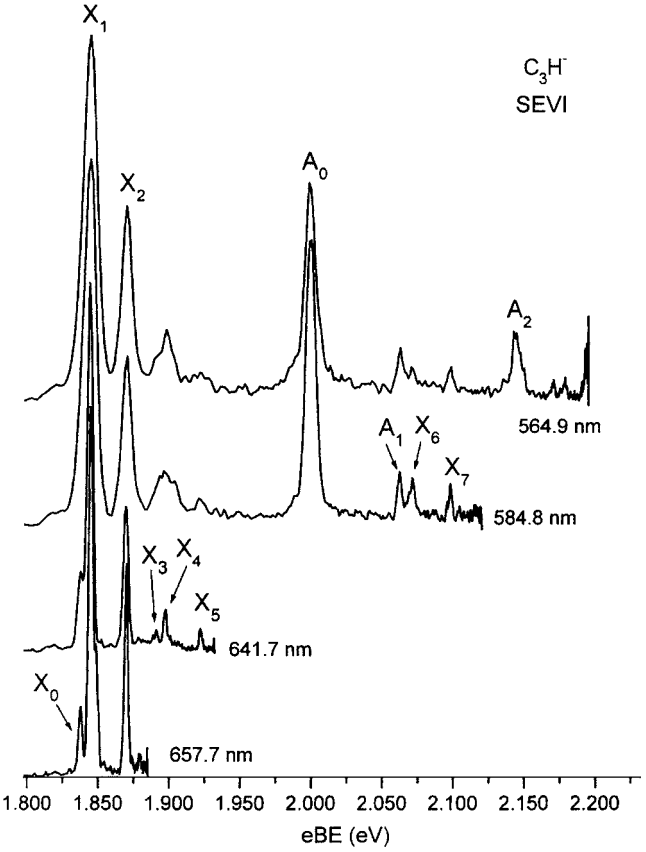


FIG. 4. SEVI photoelectron spectra of $C_3H^-$ at 657.7 (1.885 eV), 641.7 (1.932 eV), 584.8 (2.120 eV), and 564.9 (2.195 eV) nm plotted in eBE.

peaks from $C_0$ to $C_5$. Band *D* is at approximately 4.1 eV. It is only seen in the 266 nm spectrum and comprises peaks $D_0$ and $D_1$. Note that the single peak associated with band *X* and the multiple peaks assigned to band *A* have markedly different photoelectron angular distributions; the relative intensity of band *X* is considerably lower at $\theta$=0°.

Figure 2 (top) compares the 355 nm, $\theta$=90° TOF photoelectron spectra of $C_3H^-$ using acetylene (black line) and propyne (gray line, from Fig. 1) gas mixtures for the production of $C_3H^-$, as described in Sec. II. The bottom panel shows band *A* of the 355 nm, $\theta$=0° spectrum using the acetylene mix. The top panel serves to show that the relative intensities for the various bands are markedly different depending on the neutral starting material, with bands *A* and *B* considerably more intense using the acetylene mix. The bottom spectrum shows that the acetylene mix at $\theta$=0° results in an even smaller contribution from band *X*. In addition, more features from band *A*, labeled $A_0$–$A_{13}$, are resolved. Peak positions and anisotropy parameters from the photoelectron spectra in Figs. 1 and 2 are summarized in Table I.

In order to resolve bands *X* and *A* of $C_3H^-$ further, higher resolution spectra were taken in the region of 1.8–2.2 eV using the SEVI spectrometer. A typical SEVI image is shown in Fig. 3. The data were taken at 584.8 nm (2.120 eV) and show the raw symmetrized (left half) and inverse Abel-transformed (right half) image. The black arrow indicates the direction of polarization of the electric field of the laser. Figure 4 shows the resulting $C_3H^-$ photoelectron spectra from the transformed images. The plot shows data

TABLE I. Peak positions in eV, anisotropy parameters, source of the data, and vibrational and electronic assignments for the TOF spectra.

| | | TOF | | | |
|---|---|---|---|---|---|
| Peak | Energy (eV) | $\beta$ | Source | Assignment | |
| $X$ | 1.838 | −0.7 | 355 nm, propyne | ⋯ | $\tilde{A}\,^2\Pi \leftarrow \tilde{a}\,^3A''$ |
| $A_0$ | 1.998 | −0.2 | 355 nm, acetylene | $0_0^0$ | $\tilde{X}\,^2B_2 \leftarrow \tilde{X}\,^1A_1$ |
| $A_1$ | 2.057 | ⋯ | 355 nm, acetylene | $4_0^1$ | |
| $A_2$ | 2.141 | −0.3 | 355 nm, acetylene | $3_0^1$ | |
| $A_3$ | 2.199 | −0.1 | 355 nm, acetylene | $2_0^1$ | |
| $A_4$ | 2.282 | ⋯ | 355 nm, acetylene | $3_0^2$ | |
| $A_5$ | 2.347 | ⋯ | 355 nm, acetylene | $2_0^1 3_0^1$ | |
| $A_6$ | 2.405 | ⋯ | 355 nm, acetylene | $2_0^2, 3_0^3$ | |
| $A_7$ | 2.481 | ⋯ | 355 nm, acetylene | $2_0^1 3_0^2$ | |
| $A_8$ | 2.551 | ⋯ | 355 nm, acetylene | $2_0^2 3_0^1, 3_0^4$ | |
| $A_9$ | 2.611 | ⋯ | 355 nm, acetylene | $2_0^1 3_0^3, 2_0^3$ | |
| $A_{10}$ | 2.695 | ⋯ | 355 nm, acetylene | $2_0^2 3_0^2$ | |
| $A_{11}$ | 2.743 | ⋯ | 355 nm, acetylene | $2_0^3 3_0^1, 2_0^1 3_0^4$ | |
| $A_{12}$ | 2.813 | ⋯ | 355 nm, acetylene | $2_0^2 3_0^3$ | |
| $A_{13}$ | 2.881 | ⋯ | 355 nm, acetylene | $2_0^3 3_0^2, 2_0^1 3_0^5$ | |
| $B_0$ | 3.002 | 0.8 | 355 nm, propyne | $0_0^0$ | $\tilde{B}\,^2A_1 \leftarrow \tilde{X}\,^1A_1$ |
| $B_1$ | 3.072 | ⋯ | 355 nm, propyne | $3_0^1$ | |
| $C_0$ | 3.170 | 0.6 | 355 nm, propyne | $0_0^0$ | $\tilde{a}\,^4\Sigma^- \leftarrow \tilde{a}\,^3A''$ |
| $C_1$ | 3.201 | 0.5 | 355 nm, propyne | $4_0^1$ | |
| $C_2$ | 3.221 | ⋯ | 355 nm, propyne | $5_0^1$ | |
| $C_3$ | 3.232 | ⋯ | 355 nm, propyne | $4_0^2$ | |
| $C_4$ | 3.257 | 0.4 | 355 nm, propyne | $4_0^1 5_0^1, 4_0^3$ | |
| $C_5$ | 3.296 | 0.1 | 355 nm, propyne | $4_0^4$ | |
| $D_0$ | 4.115 | −0.3 | 266 nm, propyne | $0_0^0$ | $\tilde{C}\,^2A' \leftarrow \tilde{a}\,^3A''$ |
| $D_1$ | 4.157 | ⋯ | 266 nm, propyne | ⋯ | |

taken at laser wavelengths of 657.7 nm (1.885 eV), 641.7 nm (1.932 eV), 584.8 nm (2.120 eV), and 564.9 nm (2.195 eV). The two higher photon energy spectra were taken using a repeller voltage of 350 V, while the lower photon energy spectra used a repeller voltage of 250 V. The SEVI data resolve band $X$ into eight peaks, $X_0$–$X_7$, and also show several peaks belonging to band $A$, $A_0$–$A_2$. The association of peaks $X_6$ and $X_7$ with band $X$ rather than band $A$ is discussed in Sec. IV B. SEVI data were also taken for $C_3D^-$ at 655.7 nm (1.891 eV), 644.7 nm (1.923 eV), and 604.8 nm (2.050 eV) shown together in Fig. 5. Band $X'$ is analogous to band $X$ in $C_3H$ but several more peaks are apparent in the spectrum between 1.8 and 1.95 eV ($X'_0$–$X'_7$). A peak labeled $A'_0$ is also present at 1.997 eV in the 604.8 nm spectrum. The small intensity of $A'_0$ in comparison to band $X'$ is due to its proximity to threshold.[35,39] Peak positions, anisotropy parameters, and photon wavelengths from the photoelectron spectra in Figs. 4 and 5 are listed in Table II.

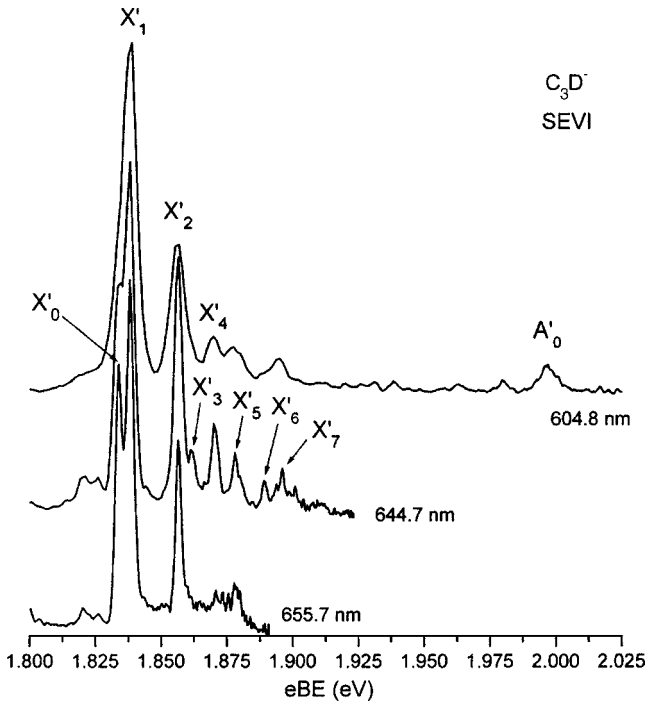


FIG. 5. SEVI photoelectron spectra of $C_3D^-$ at 655.7 (1.891 eV), 644.7 (1.923 eV), and 604.8 (2.050 eV) nm plotted in eBE.

## B. Electronic structure calculations

Electronic structure calculations were performed on neutral and anionic $c$-$C_3H$ and $l$-$C_3H$. There have been many previous studies on the structure and energetics of $C_3H$ and its anion, and the purpose of the current calculations is not improve upon these, but to reproduce the representative force constants for each state in order to simulate FC factors and

TABLE II. Peak positions in eV, anisotropy parameters, source of the data, and vibrational and electronic assignments for the SEVI spectra.

| | SEVI | | | | |
|---|---|---|---|---|---|
| Peak | Energy (eV) | $\beta$ | Source | Assignment | |
| $X_0$ | 1.838 | −0.5 | 657.7 nm | $4_1^1$ $(K=0\leftarrow K'=1)$ | |
| $X_1$ | 1.844 | −0.7 | 657.7 nm | $0_0^0$ $(K=1\leftarrow K'=0)$ | $\tilde{A}\,^2\Pi\leftarrow\tilde{a}\,^3A''$ |
| $X_2$ | 1.870 | −0.5 | 641.7 nm | ⋯ | |
| $X_3$ | 1.891 | ⋯ | 641.7 nm | ⋯ | |
| $X_4$ | 1.898 | −0.3 | 641.7 nm | ⋯ | |
| $X_5$ | 1.922 | ⋯ | 641.7 nm | ⋯ | |
| $X_6$ | 2.072 | ⋯ | 584.5 nm | $2_0^1$ | |
| $X_7$ | 2.098 | ⋯ | 584.5 nm | ⋯ | |
| $A_0$ | 1.999 | −0.3 | 584.5 nm | $0_0^0$ | $\tilde{X}\,^2B_2\leftarrow\tilde{X}\,^1A_1$ |
| $A_1$ | 2.062 | 1.1 | 584.5 nm | $4_0^1$ | |
| $A_2$ | 2.143 | −0.1 | 564.9 nm | $3_0^1$ | |
| $X'_0$ | 1.834 | −0.1 | 655.7 nm | $4_1^1$ $(K=0\leftarrow K'=1)$ | |
| $X'_1$ | 1.838 | −0.2 | 655.7 nm | $0_0^0$ $(K=1\leftarrow K'=0)$ | $\tilde{A}\,^2\Pi\leftarrow\tilde{a}\,^3A''$ |
| $X'_2$ | 1.857 | −0.2 | 655.7 nm | ⋯ | |
| $X'_3$ | 1.861 | ⋯ | 644.7 nm | ⋯ | |
| $X'_4$ | 1.870 | ⋯ | 644.7 nm | ⋯ | |
| $X'_5$ | 1.878 | ⋯ | 644.7 nm | ⋯ | |
| $X'_6$ | 1.889 | ⋯ | 644.7 nm | ⋯ | |
| $X'_7$ | 1.896 | ⋯ | 644.7 nm | ⋯ | |
| $A'_0$ | 1.997 | ⋯ | 604.8 nm | $0_0^0$ | $\tilde{X}\,^2B_2\leftarrow\tilde{X}\,^1A_1$ |

TABLE III. Calculated geometries and vibrational frequencies from current and previous calculations and experiment. $c$-$C_3H$ vibrational modes: $\nu_1(a_1)$ CH stretch, $\nu_2(a_1)$ sym. ring stretch, $\nu_3(a_1)$ scissor, $\nu_4(b_2)$ asym. ring distortion, $\nu_5(b_2)$ CH wag, $\nu_6(b_1)$ CH wag (out of plane), $l$-$C_3H$ vibrational modes: $\nu_1(\sigma/a')$ CH stretch, $\nu_2(\sigma/a')$ CCC asym. stretch, $\nu_3(\sigma/a')$ CCC sym. stretch, $\nu_4(\pi/a')$ CCH bend, $\nu_5(\pi/a')$ CCH bend, $\nu_6(a'')$ CCC bend (out of plane).

| $c$-$C_3H$ | | $r(HC_1)$ | $r(C_1C_2)$ | $r(C_2C_3)$ | $\alpha(HC_1C_2)$ | $\alpha(C_1C_2C_3)$ | $\nu_1(a_1)$ | $\nu_2(a_1)$ | $\nu_3(a_1)$ | $\nu_4(b_2)$ | $\nu_5(b_2)$ | $\nu_6(b_1)$ |
|---|---|---|---|---|---|---|---|---|---|---|---|---|
| $^1A_1$ | B3LYP/aug-cc-pVTZ[a] | 1.088 | 1.371 | 1.483 | 147.2 | 57.2 | 3049 | 1523 | 898 | 1299 | 864 | 852 |
| | CCSD(T)/aug-cc-pVQZ[b] | 1.083 | 1.380 | 1.507 | 146.9 | 56.9 | 3101 | 1503 | 890 | 1287 | 859 | 968 |
| $^2B_2$ | B3LYP/aug-cc-pVTZ[a] | 1.079 | 1.369 | 1.361 | 150.2 | 60.2 | 3222 | 1616 | 1236 | 578 | 921 | 879 |
| | EOMIP-CCSD/PVTZ[c] | 1.070 | 1.367 | 1.367 | 150.0 | 60.0 | 3330 | 1639 | 1244 | 281 | 958 | 898 |
| | MP2/6-31G$(d,p)$[d] | 1.079 | 1.375 | 1.388 | 149.7 | 59.7 | 3325 | 1657 | 1206 | 12526 | 969 | 877 |
| | Expt.—microwave[e] | 1.076 | 1.374 | 1.377 | 149.9 | 59.9 | ⋯ | ⋯ | ⋯ | 508 | ⋯ | ⋯ |
| $^2A_1$ | B3LYP/aug-cc-pVTZ[a] | 1.079 | 1.366 | 1.531 | 145.9 | 55.9 | 3210 | 1526 | 734 | 2747 | 859 | 822 |
| | EOMIP-CCSD/PVTZ[e] | 1.070 | 1.366 | 1.515 | 146.3 | 56.3 | 3316 | 1567 | 831 | 2155 | 891 | 854 |
| $l$-$C_3H$ | | | | | | | $\nu_1(\sigma/a')$ | $\nu_2(\sigma/a')$ | $\nu_3(\sigma/a')$ | $\nu_4(\pi/a')$ | $\nu_5(\pi/a')$ | $\nu_6(a'')$ |
| $^3\Sigma^-$ | B3LYP/aug-cc-pVTZ[a] | 1.059 | 1.275 | 1.316 | 180.0 | 180.0 | 3456 | 1670 | 1182 | 457i | 427 | ⋯ |
| $^3A''$ | B3LYP/aug-cc-pVTZ[a] | 1.073 | 1.296 | 1.303 | 143.4 | 175.2 | 3272 | 1664 | 1190 | 613 | 396 | 427 |
| | CASSCF/D95$v^{**}$[f] | 1.071 | 1.318 | 1.321 | 137.7 | 172.6 | 3417 | 1553 | 1200 | 791 | 411 | 434 |
| $^2\Pi$ | B3LYP/aug-cc-pVTZ[a] | 1.064 | 1.240 | 1.330 | 180.0 | 180.0 | 3436 | 1904 | 1177 | 197i/831 | 246/381 | ⋯ |
| $^2A'$ | B3LYP/aug-cc-pVTZ[a] | 1.067 | 1.247 | 1.325 | 160.6 | 176.1 | 3397 | 1892 | 1192 | 256 | 376 | 243 |
| | CCSD(T)/TZP[g] | 1.072 | 1.253 | 1.336 | 156.5 | 174.0 | 3380 | 1876 | 1170 | 351 | 368 | 208 |
| | Expt.—matrix FTIR[h] | ⋯ | ⋯ | ⋯ | ⋯ | ⋯ | 3238 | 1825 | 1160 | ⋯ | ⋯ | ⋯ |
| $^4\Sigma^-$ | B3LYP/aug-cc-pVTZ[a] | 1.061 | 1.253 | 1.285 | 180.0 | 180.0 | 3449 | 1726 | 1288 | 263 | 437 | ⋯ |

[a]This work.
[b]Reference 27.
[c]Reference 12.
[d]Reference 15.
[e]Reference 23.
[f]Reference 25.
[g]Reference 16.
[h]Reference 19.

TABLE IV. Relative energies in eV for the anion and neutral states of $C_3H$. The lowest energy cyclic isomer serves as the reference energy in both the anion and neutral manifolds. Relative energies including zero-point energies are listed in parentheses where available.

| | Anion | | | Neutral | | |
|---|---|---|---|---|---|---|
| Level/basis set | $^1A_1$ | $^3\Sigma^-$ | $^3A''$ | $^2B_2$ | $^2\Pi$ | $^2A''$ |
| B3LYP/aug-cc-pVTZ[a] | 0 | 0.092 (0.011) | 0.028 (–0.029) | 0 | 0.033 (0.003) | 0.030 (–0.038) |
| SDCI+Q/[5s3p2d1f/3s2p1d][b] | 0 | 0.252 (0.161) | 0.221 (0.182) | ⋯ | ⋯ | ⋯ |
| CCSD(T)/6-311++G(2d,p)[b] | 0 | 0.303 (0.213) | 0.191 (0.152) | ⋯ | ⋯ | ⋯ |
| MRCI/Q/aug-cc-pVTZ[c] | 0 | 0.310 | ⋯ | 0 | 0.049 | ⋯ |
| RCCSD(T)/aug-cc-pVTZ[c] | 0 | 0.425 | ⋯ | 0 | 0.118 | ⋯ |
| CASSCF/D95(d,p)[d] | ⋯ | ⋯ | ⋯ | 0 | 0.065 (0.087) | –0.022 (–0.048) |
| MRCI+Q/VTZ(2df,2p)[d] | ⋯ | ⋯ | ⋯ | 0 | 0.084(0.044) | 0.068(–0.021) |
| CCSD(T)/QZ2P[e] | ⋯ | ⋯ | ⋯ | 0 | 0.143 | 0.150 |
| CCSD(T)/cc-pVQZ[e] | ⋯ | ⋯ | ⋯ | 0 | 0.135 (0.074) | 0.143 (0.081) |

[a]This work.
[b]Reference 25.
[c]Reference 26.
[d]Reference 15.
[e]Reference 16.

interpret the photoelectron spectra. Density functional calculations were performed using the Becke three-parameter Lee-Yang-Parr exchange-correlation functional[40,41] (B3LYP) along with the augmented correlation consistent polarized valence triple-$\zeta$ basis set[42] (aug-cc-pVTZ). All computations were performed using the GAUSSIAN03 program.[43] Table III summarizes our calculated optimized geometries and vibrational frequencies and compares them to other calculations and previous experimental values. Table IV shows calculated energetics of the anion and neutral. Table V shows calculated transition energies, as well as those of several theoretical and experimental studies. Figure 6 provides a schematic overview of the states of *l*-$C_3H$ and *c*-$C_3H$ with their calculated B3LYP structures; the energetics derive from a mixture of theory and experiment as discussed in Sec. IV.

TABLE V. Calculated and experimental transition energies between selected states of linear and cyclic $C_3H$. Transitions indicated with an asterisk can be directly observed in the photoelectron spectra, while the remaining ones are neutral-neutral transitions.

| Transition | ΔZPE (eV) | Method |
|---|---|---|
| | *c*-$C_3H$ | |
| $^1A_1 \rightarrow {}^2B_2{}^*$ | 1.940 | B3LYP/aug-cc-pVTZ[a] |
| | 1.999±0.003 | Expt.—PES[a] |
| | 1.963 | Expt.—PES[b] |
| | 2.012 | RCCSD(T)/aug-cc-pVTZ[c] |
| | 1.89 | SDCI+Q/[5s3p2d1f/3s2p1d][d] |
| $^2B_2 \rightarrow {}^2A_1$ | 1.009 | B3LYP/aug-cc-pVTZ[a] |
| | 1.003±0.012 | Expt.—PES[a] |
| | 1.011 | EOMIP-CCSD/TZ2P[e] |
| | 1.339 | Est. from microwave data[f] |
| | *l*-$C_3H$ | |
| $^3A'' \rightarrow {}^2\Pi^*$ | 1.931 | B3LYP/aug-cc-pVTZ[a] |
| | 1.844±0.003 | Expt.—PES[a] |
| | 1.858±0.027 | Expt.—PES[g] |
| | 1.847±0.012 | Expt.—photodetachment[h] |
| $^2\Pi \rightarrow {}^4\Sigma^-$ | 1.415 | B3LYP/aug-cc-pVTZ[a] |
| | 1.326±0.018 | Expt.—PES[a] |
| | 1.17 | MCCEPA/aug-cc-pVTZ[i] |
| $^2\Pi \rightarrow {}^2A'$ ($^2\Delta$) | 2.271±0.023 | Expt.—PES[a] |
| | 2.05 | CASSCF/aug-cc-pVTZ[j] |
| | 2.379 | Expt.—R2C2PI[j] |
| $^2\Pi \rightarrow {}^2A''$ ($^2\Delta$) | 2.22 | CASSCF/aug-cc-pVTZ[j] |
| | 2.546 | Expt.—R2C2PI[j] |

[a]This work.
[b]Reference 32.
[c]Reference 26.
[d]Reference 11.
[e]Reference 12.
[f]Reference 23.
[g]Reference 31.
[h]Reference 29.
[i]Reference 30.
[j]Reference 20.

### 1. Anions

The optimized geometries and vibrational frequencies of the lowest lying cyclic ($^1A_1$), linear ($^3\Sigma^-$), and bent ($^3A''$) states of the anion were calculated. The electronic configuration of the $^1A_1$ state is $\ldots(1b_1)^2(6a_1)^2(3b_2)^2$, while that of the $^3\Sigma^-$ linear state is $\ldots(1\pi)^4(7\sigma)^2(2\pi_x)^1(2\pi_y)^1$, which upon bending correlates to the $^3A''$ electronic configuration $\ldots(7a')^2(1a'')^2(8a')^2(9a')^1(2a'')^1$. Lakin *et al.*[27] predicted the cyclic $^1A_1$ state to be a stable minimum on the anion potential energy surface with a high barrier to isomerization (~2 eV) at the CCSD(T) level of theory. Our B3LYP calculations accurately reproduce Lakin's CCSD(T)/aug-cc-pVQZ structure and frequencies. The $^3\Sigma^-$ state is a transition state, as seen by the imaginary frequencies for the degenerate $\nu_4$ bending mode. For the $^3A''$ state, the calculated B3LYP geometry matches up fairly well to the CASSCF calculation of Aoki *et al.*[25] The frequencies also match up well with the exception of $\nu_4$, which is off by approximately 23%. This discrepancy presumably reflects the fact that the potential energy function along the corresponding bending coordinate is not very harmonic and is better represented by a double minimum potential with a fairly small barrier, for which calculated[25] and experimental[29,30] values range from 244 to 950 $cm^{-1}$. Our B3LYP calculations give an intermediate value of 524 $cm^{-1}$.

Table IV summarizes the energetics of the anionic states obtained in our calculations and in previous work. Note that

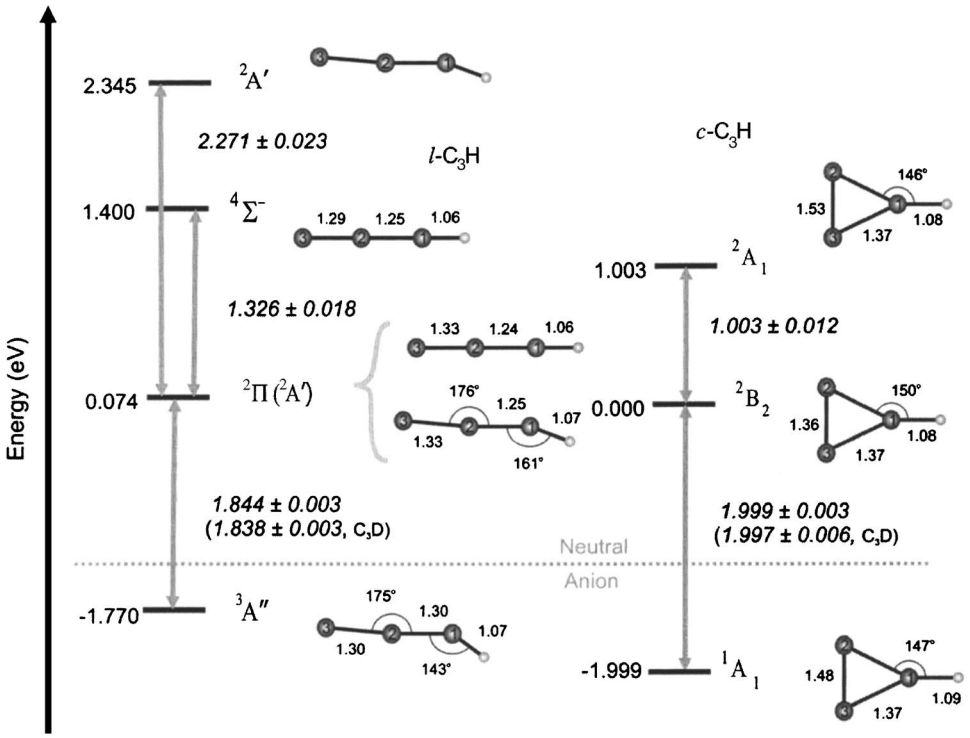


FIG. 6. Schematic overview of the electronic states of $C_3H$ along with the B3LYP/aug-cc-pVTZ structures where available. The energy scale is referenced to the neutral ground state. Since no linear to cyclic or vice-versa transitions are observed, the energy splitting of the lowest lying neutral linear and cyclic isomers is taken from Ref. 16. All other energy separations are from experiment.

all calculations reported to date predict that the $^1A_1$ state of $c$-$C_3H^-$ is the global minimum. It lies slightly below the $^3A''$ state of $l$-$C_3H^-$, with the spacing depending on the level of theory used.

### 2. Neutrals

Geometries, frequencies, and energetics for five states of neutral $C_3H$ were calculated. Table III shows the structures and frequencies for the ground ($^2B_2$) and first excited ($^2A_1$) states of the cyclic isomer, as well as the $^2A'$, $^2\Pi$, and $^4\Sigma^-$ states of $l$-$C_3H$. Upon photodetachment of a $3b_2$ electron from the $^1A_1$ cyclic anion, the electronic configuration becomes that of the $^2B_2$ cyclic neutral state: $\ldots(5a_1)^2(1b_1)^2(6a_1)^2(3b_2)^1$. For $l$-$C_3H$, detachment from the $2\pi(2a'')$ orbital in the $^3\Sigma^-(^3A'')$ state leads to the electron configuration $\ldots(1\pi)^4(7\sigma)^2(2\pi)^1$ $[\ldots(7a')^2(1a'')^2(8a')^2(9a')^1]$ for the $^2\Pi(^2A')$ state. Detachment from the next lowest $7\sigma(9a')$ orbital leads to the electronic configuration $\ldots(1\pi)^4(7\sigma)^1(2\pi_x)^1(2\pi_y)^1$ of the $^4\Sigma^-$ excited state.

For $c$-$C_3H$, the calculated $^2B_2$ and $^2A_1$ geometries match up well to the EOIMP-CCSD calculations of Stanton,[12] the MP2 calculations of Takahashi and Yamashita,[15] and the structure of the lowest energy $^2B_2$ state obtained from microwave spectroscopy.[23] Additionally, with the exception of the $\nu_4$ modes of both states, the frequencies are very well reproduced. The $\nu_4$ mode corresponds to an asymmetric ring stretching mode which lowers the symmetry of the molecule from $C_{2v}$ to $C_s$. The difficulty in calculating frequencies for this mode arises from a pseudo-Jahn-Teller interaction between the $^2B_2$ ground state and the $^2A_1$ first excited state, which perturbs the potential surfaces along the $\nu_4$ coordinate. From microwave data, Yamamoto and Saito[23] estimated the $\nu_4$ frequency to be 508 $cm^{-1}$, which compares favorably to our B3LYP frequency of 578 $cm^{-1}$, although this agreement may be fortuitous.

For $l$-$C_3H$, our B3LYP calculations find the bent $^2A'$ state to be a true minimum with a very low frequency of 256 $cm^{-1}$ for the $\nu_4$ mode, essentially a CCH bending mode. The $^2\Pi$ state is a transition state with one imaginary frequency for $\nu_4$. The linear geometry is only 4 meV above the minimum for the $^2A'$ state. Our calculations thus suggest a single state with a very flat CCH bending potential. These results are consistent with previous calculations[15,16] that showed the linear and bent structures lying very close to one another. For example, Ochsenfeld *et al.*[16] found the bent structure to be 11 meV below the linear geometry at the CCSD(T) level of theory using a TZP basis set, but with increasing basis set the situation reverses and the linear isomer becomes 8 meV lower in energy (cc-pVQZ basis set). We shall therefore refer to the ground state of $l$-$C_3H$ using the $^2\Pi$ term symbol with the expectation that it is quasilinear, consistent with microwave data[24] and the previous theoretical treatment by Perić *et al.*,[14,44] who considered Renner-Teller and spin-orbit effects in $l$-$C_3H$. The higher-lying linear $^4\Sigma^-$ state does not suffer from these complications; our results are the first calculated structures and frequencies are reported in the literature.

Table IV also lists the energetics calculated in this and previous work for the lowest lying $l$-$C_3H$ and $c$-$C_3H$ isomers. As was the case in the anion, these isomers are very close in energy with $c$-$C_3H$ being slightly more stable. At the highest level of theory reported to date, Ochsenfeld *et al.*[16] found the equilibrium geometry of $c$-$C_3H$ to lie 135 meV below that of $l$-$C_3H$; this difference is reduced to 74 meV when zero-point energies are included.

## IV. DISCUSSION

### A. Band assignments

The progression of peaks comprising bands *X* and *A* in Fig. 1 exhibits a profile similar to that observed in the previous photoelectron spectrum by Oakes and Ellison.[31] They used a simple generalized valence bond model to predict linear structures for both the anion and neutral and assigned the progression to a single mode of the linear isomer with a frequency of 1120 $cm^{-1}$, close to the $X-A_0-A_2$ peak spacing in our spectra of about 1200 $cm^{-1}$. However, Table V shows that the calculated photodetachment transition energy between the cyclic anion and neutral ground states is virtually identical to the corresponding energy between the linear isomers, raising the possibility of overlapping transitions from the two isomers in this spectral region.

The current work strongly supports assignment to two distinct bands. Table I shows that the anisotropy parameter for band *X* is considerably more negative than for the peaks comprising band *A*; this result is also evident by visual inspection of the 355 nm PE spectra in Fig. 1. Hence, band *X* involves transitions between different electronic states than band *A*. Further insight comes from the top panel in Fig. 2, which compares PE spectra of $C_3H^-$ using acetylene and propyne as described previously. Compared to bands *A* and *B*, bands *X* and *C* are considerably more intense when propyne is used as the precursor. *X* and *A* are thus assigned as two distinct bands arising from two different isomers of $C_3H^-$ and not as part of the same progression. The *X* and *C* bands appear to belong to one isomer, while the *A* and *B* bands arise from a second isomer. Given that propyne already has a linear $C_3$ backbone, the enhanced intensity of bands *X* and *C* when using propyne as the starting material supports assignment of both bands to transitions originating from the $^3A''$ state of $l$-$C_3H^-$, and bands *A* and *B* to photodetachment from the $^1A_1$ state of $c$-$C_3H^-$.

Using energetics from current and previous calculations and previous experimental values (Table V), all the observed bands in the 355 and 266 nm TOF spectra, *X* through *D*, can be assigned to specific transitions of $l$-$C_3H$ and $c$-$C_3H$. Band *X* is assigned to the $^2\Pi \leftarrow {}^3A''$ transition, i.e., the transition between the lowest lying states of $l$-$C_3H$ and $l$-$C_3H^-$. The binding energy of band *X* in the 355 nm spectrum gives an approximate value of 1.84 eV for this transition; a more precise determination from FC simulations will be given in the next section. In any case, this experimental energy agrees with the lowest energy feature seen in the previous photoelectron spectrum by Oakes and Ellison (1.858±0.027 eV),[31] which was also assigned to the transition between linear isomers of the anion and neutral, and the energy obtained by Pachkov *et al.* 1.847±0.012 eV, for the photodetachment threshold of this transition.[29]

Band *A* is assigned as the transition from the cyclic $^1A_1$ anion state to the $^2B_2$ neutral state. Peak $A_0$ appears to be the vibrational origin of this transition at eBE=1.999 eV, as measured in the SEVI spectrum of Fig. 4. Using this value in Fig. 6, and assuming the relative energetics for the ground vibrational states of neutral $c$-$C_3H$ and $l$-$C_3H$ calculated by Ochsenfeld *et al.*[16] are correct, the eBE's of $X_1$ and $A_0$ place the ground vibrational state of $c$-$C_3H^-$ below that of $l$-$C_3H^-$ by 229 meV. These assignments, supported by the analysis below, confirm the consensus theoretical result that $c$-$C_3H^-$ is the lower energy isomer of the anion. Hence, peak $A_0$ is the vibrational origin of the $\tilde{X}\,^2B_2 \leftarrow \tilde{X}\,^1A_1$ transition and its eBE is the adiabatic EA of $C_3H$. Note that we cannot experimentally fix the manifold of photodetachment transitions within the cyclic manifold with respect to those in the linear/bent manifold since no transitions between the two classes of isomers are seen in the photoelectron spectra. The only way that $l$-$C_3H^-$ could be the anion ground state is if neutral $l$-$C_3H$ lies 155 meV or more below neutral $c$-$C_3H$, which is at variance with all calculations on this species. We henceforth refer to the lowest states of $l$-$C_3H^-$ and $l$-$C_3H$ as the $\tilde{a}\,^3A''$ and $\tilde{A}\,^2\Pi$ states, respectively.

Band *B* in both the 355 and 266 nm spectra is dominated by a single intense peak, indicating a small geometry change between the initial and final states. Peak $B_0$ appears at 3.002 eV in both spectra. It is separated from *X* by 1.16 eV and from $A_0$ by 1.004 eV. Based solely on energetics, $B_0$ can be assigned as the vibrationless transition from the anion ground state to the first excited state of either $l$-$C_3H(\tilde{a}\,^4\Sigma^- \leftarrow \tilde{a}\,^3A'')$ or $c$-$C_3H(\tilde{B}\,^2A_1 \leftarrow \tilde{X}\,^1A_1)$. The transition energies between the lowest lying $l$-$C_3H$ and $c$-$C_3H$ states (Table V) were calculated to be 1.415 and 1.009 eV, respectively. However, since band *B* is more intense when the acetylene mix is used, we associate it with the cyclic manifold of transitions. The $^2A_1$ state is calculated to be very similar in geometry to the $^1A_1$ anion ground state (the largest bond length change is 0.05 Å) and would more likely exhibit a single sharp peak. These qualitative arguments are further supported by spectral simulations in Sec. IV B. Band *B* is therefore assigned as the transition to the first cyclic excited state, $\tilde{B}\,^2A_1 \leftarrow \tilde{X}\,^1A_1$.

Band *C* is expected to belong to a transition involving $l$-$C_3H$. It comprises several intense features ($C_0$, $C_1$, $C_4$, and $C_5$) in the 355 nm spectra (Fig. 1). The less intense peaks ($C_2$ and $C_3$) can be seen in an expanded view of band *C* in the inset of the top panel in Fig. 1. Peak $C_0$ is assigned as the band origin with an eBE of 3.17 eV. It lies 1.326 eV above the most intense feature in the lowest lying $l$-$C_3H$ state, which is close to the B3LYP (1.415 eV) and MCCEPA [1.17 eV (Ref. 30)] values for the $^2\Pi \rightarrow {}^4\Sigma^-$ transition energies (Table V). Although it is partially cut off in the 355 nm spectrum, the band is fairly extended indicating a large change in geometry. Band *C* is therefore assigned as the $\tilde{a}\,^4\Sigma^- \leftarrow \tilde{a}\,^3A''$ transition.

A fifth band is accessed in the 266 nm spectrum beyond the 355 nm cutoff. Band *D* is relatively intense in the TOF spectrum using propyne (Fig. 1), but is much less intense in the 266 nm acetylene spectrum (not shown), suggesting that it originates from $l$-$C_3H^-$. The main peak $D_0$ is expected to be the band origin at 4.115 eV eBE corresponding to an energy of 2.271 eV above the $^2\Pi$ state. This value is closest in energy to the theoretical and experimental values of 2.05 and 2.379 eV, respectively, found by Ding *et al.*[20] for the $\tilde{C}\,^2A' \leftarrow \tilde{A}\,^2\Pi$ transition in $C_3H$. Ding *et al.* pointed out that, owing to the large geometry change, the assigned origin for

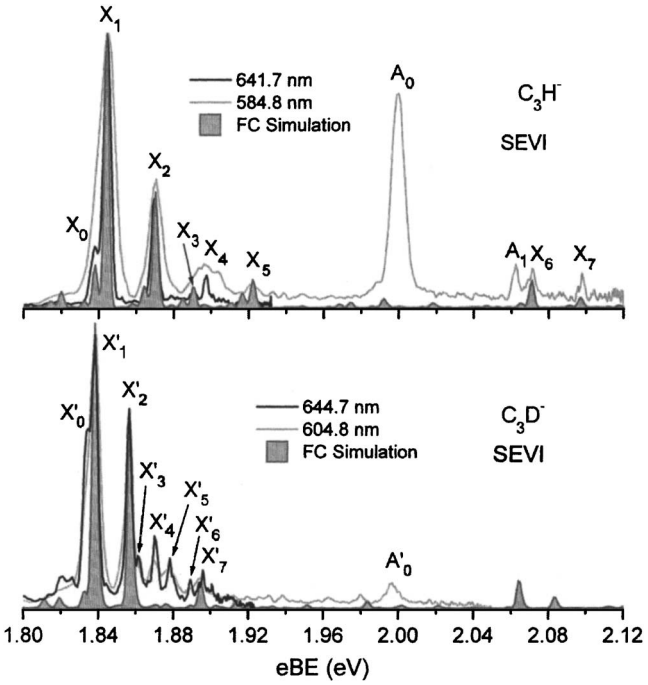


FIG. 7. TOP: Franck-Condon simulation of band $X$ (gray fill) overlapped with the 641.7 nm (black trace) and 584.8 nm (light gray trace) SEVI spectra. BOTTOM: Franck-Condon simulation of band $X'$ (gray fill) overlapped with the 644.7 nm (black trace) and 604.8 nm (light gray trace) SEVI spectra.

this transition was quite weak and the true origin might not have been observed, so that their reported value is an upper bound. They also found a much stronger origin for the $\tilde{D}\,^2A'' \leftarrow \tilde{A}\,^2\Pi$ band at 2.547 eV, a higher term energy than implied by band $D$. Note that the $\tilde{C}\,^2A'$ and $\tilde{D}\,^2A''$ bent states correlate to a linear $^2\Delta$ state. In any case, comparison to these results supports assignment of band $D$ in our PE spectra to the $\tilde{C}\,^2A' \leftarrow \tilde{a}\,^3A''$ photodetachment transition.

### B. Franck-Condon simulations and vibrational assignments

To gain further insight into the photoelectron spectra, FC simulations were used in conjunction with our electronic structure calculations. The simulations were carried out treating each mode as an independent harmonic oscillator including the effects of Duschinsky rotation[45] between all modes. The FCFGAUS program of Ervin *et al.* was used to extract the Duschinsky rotation matrix and normal coordinate displacement vector from the GAUSSIAN03 output. These values as well as the vibrational temperature (300 K was used for all simulations) and anion and neutral vibrational frequencies were then used as input into the PESCAL program,[46,47] which calculates FC factors and outputs the simulated spectrum.

FC simulations were undertaken for four bands of $C_3H$ and one band of $C_3D$: $\tilde{A}\,^2\Pi \leftarrow \tilde{a}\,^3A''$ (bands $X$ and $X'$), $\tilde{X}\,^2B_2 \leftarrow \tilde{X}\,^1A_1$ (band $A$), $\tilde{B}\,^2A_1 \leftarrow \tilde{X}\,^1A_1$ (band $B$), and $\tilde{a}\,^4\Sigma^- \leftarrow \tilde{a}\,^3A''$ (band $C$) to confirm their assignments and extract vibrational information. Band $D$ was not simulated owing to the absence of structural and vibrational calculations. Bands $A$, $B$, and $C$ were simulated using the 355 nm TOF spectra for comparison, while $X$ and $X'$ were simulated using the higher resolution SEVI spectra. Simulations involving the cyclic isomer, bands $A$ and $B$ (Figs. 1 and 2), were relatively straightforward, while attempts at simulating $l$-$C_3H$ transitions, bands $X$, $X'$, and $C$ (Figs. 1 and 7), were more problematic owing to the anharmonic nature of one of the active modes, namely, the $\nu_4$ HCC bending mode. Bands $X$ and $X'$ were particularly averse to harmonic vibrational analysis because of the strong Renner-Teller interactions expected for the neutral $\tilde{A}\,^2\Pi$ state. For this reason, we consider the $c$-$C_3H$ transitions first, and then the simulations of $l$-$C_3H/C_3D$.

#### 1. $c$-$C_3H$

Figure 2, bottom, compares the 355 nm spectrum of $C_3H^-$ made from acetylene with the stick and convoluted FC simulations of band $A$. Table I gives peak assignments from the simulation. The B3LYP calculations were used as starting points for the fit. The origin of the simulation was shifted to match $A_0$, the expected origin of band $A$. With only slight adjustment from calculations, the simulation matches the band profile band quite well, and all major peaks except $A_1$ are reproduced. Since both the cyclic anion and neutral ground states are predicted to have $C_{2v}$ symmetry, only completely symmetric $(a_1)$ vibrational modes should be active in the absence of vibronic coupling. Peak $A_2$ is assigned to the first quanta of the $\nu_3(a_1)$ $C_2-C_3$ scissoring mode of the neutral with a frequency of $1161\pm25$ cm$^{-1}$. The observed frequency is somewhat lower than the calculated frequencies at the B3LYP (1236 cm$^{-1}$) and EOMIP-CCSD (1244 cm$^{-1}$) levels of theory. Peak $A_3$ is assigned to the first quanta of the $\nu_2(a_1)$ ring stretching mode of the neutral with a frequency of $1613\pm25$ cm$^{-1}$. The B3LYP frequency (1616 cm$^{-1}$) is in excellent agreement, however, the EOMIP-CCSD and MP2 values (1639 and 1657 cm$^{-1}$, respectively) are slightly higher. Peaks $A_4-A_{13}$ are assigned to overtones and combination bands of $\nu_2$ and $\nu_3$ or combinations thereof, with assignments listed in Table I. The FC simulation confirms the assignment of band $A$ to $\tilde{X}\,^2B_2 \leftarrow \tilde{X}\,^1A_1$ with $A_0$ as the origin, and from the position of peak $A_0$ in the SEVI spectrum at 548.4 nm we find $EA(C_3H)=1.999\pm0.003$ eV, as mentioned in Sec. IV A. The $C_3D$ SEVI spectra also show the origin of the $A'$ band, yielding $EA(C_3D)=1.997\pm0.005$ eV. Figure 6 shows EAs as well as other experimental energy differences obtained by the spectra for $l$-$C_3H$ and $c$-$C_3H$.

Peak $A_1$ is prominently absent in the FC simulation of band $A$. This peak lies 508 cm$^{-1}$ from $A_0$, as seen in the SEVI spectrum, a value identical to the estimated $\nu_4$ fundamental for the $\tilde{X}\,^2B_2$ state from the microwave spectrum of $c$-$C_3H$ by Yamamoto and Saito,[23] suggesting that it be assigned to the $4_0^1$ transition. As discussed by Stanton,[12] the $\nu_4$ mode, with $b_2$ symmetry, experiences pseudo-Jahn-Teller coupling with the nearby $\tilde{B}\,^2A_1$ excited state. The appearance of peak $A_1$ in the photoelectron spectrum but not the FC simulation is consistent with such a vibronic coupling effect, which is well known to result in nominally forbidden transitions appearing in a photoelectron spectrum.[48,49] We also note that the photoelectron angular distribution of peak $A_1$, as

seen in the SEVI image in Fig. 3, is considerably more anisotropic than that of the neighboring peaks $A_0$ and $A_2$, as evidenced by its considerably more positive anisotropy parameter (see Table II). This positive anisotropy parameter is more characteristic of band $B$ (Table I), assigned above to photodetachment to the $\tilde{B}\,^2A_1$ state, providing additional evidence that peak $A_1$ results from vibronic coupling to that state.[50,51]

The simulation of band $B$ is shown in the inset in the top panel of Fig. 1 and consists of only two significant peaks. Due to the small geometry change calculated between the anion ground state and the $\tilde{B}\,^2A_1$ state of $c$-$C_3H$, only the $\nu_3(a_1)$ $C_2$–$C_3$ scissoring mode with a frequency of 734 $cm^{-1}$ shows any noticeable activity in the simulation. Though it is separated from $B_0$ by only 565 $cm^{-1}$, $B_1$ appears to be the only candidate for the $3_0^1$ transition within this band, suggesting that our calculated vibrational frequency is too high. Given $B_0$ as the origin of band $B$ and using the SEVI value for the EA for the ground state, the term energy the $\tilde{B}\,^2A_1$ state is measured to be $1.003 \pm 0.012$ eV.

### 2. *l*-$C_3H$

We next consider bands $X/X'$ and $C$, which have been assigned to transitions between the bent $\tilde{a}\,^3A''$ state of $l$-$C_3H^-/C_3D$ and the linear (or quasilinear) $\tilde{A}\,^2\Pi$ and $\tilde{a}\,^4\Sigma^-$ states of $l$-$C_3H/C_3D$, respectively. Based on the calculated geometries (see Table III and Fig. 6), one expects the primary vibrational activity in both bands to be in the CCH $\nu_4$ bending mode. There is experimental and theoretical evidence that this mode involves large amplitude motion in both the anion and neutral, complicating simulation of these bands by standard harmonic analysis. For example, as mentioned previously, the bent $^3A''$ anion ground state has an approximately symmetric, double-well HCC bend potential with a relatively low barrier to linearity; calculated barrier heights range from 244 [SDCl+Q (Ref. 11)] to 909 $cm^{-1}$ [CCSD(T) (Ref. 16)]. The neutral $\tilde{A}\,^2\Pi$ state exhibits strong Renner-Teller coupling in the $\nu_4$ mode,[14,22] resulting in sufficiently large amplitude bend motion so that the vibrationally averaged C–H bond distance, as measured by microwave spectroscopy,[24] is noticeably shorter than in a "normal" linear molecule (1.0171 versus 1.0605 Å in $C_2H_2$). Finally, the neutral $^4\Sigma^-$ state, while linear, may have a very flat and therefore anharmonic bend potential.[30] In spite of these considerations, it is useful to simulate these bands using standard methods in order to see which features can be assigned and which require further analysis.

First, consider band $X$ in the $C_3H$ SEVI spectra, which appears to be dominated by a single progression consisting of peaks $X_1$, $X_2$, $X_4$, and $X_5$ with an average spacing of 210 $cm^{-1}$. The $X_1$-$X_2$ spacing is 210 $cm^{-1}$, the $X_2$-$X_4$ spacing is 226 $cm^{-1}$, and the $X_4$-$X_5$ spacing is 194 $cm^{-1}$. This spacing is close to the calculated B3LYP frequency of 256 $cm^{-1}$ for the HCC bend for the $^2A'$ structure (see Table III). A harmonic FC simulation of band $X$ with slight adjustments of frequency and geometry is overlaid on the experimental spectrum in Fig. 7. Somewhat surprisingly, this simulation reproduces nearly all the peaks in the spectrum, with the exception of $X_4$, which has no intensity in the simulation. On the basis of this simulation, we would assign peaks $X_1$, $X_2$, $X_4$, and $X_5$ as a $4_0^n$ progression with $\nu_4 = 210 \pm 10$ $cm^{-1}$, $X_3$ as the $5_0^1$ transition with $\nu_5 = 376 \pm 10$ $cm^{-1}$, $X_6$ as the $2_0^1$ transition with $\nu_2 = 1839 \pm 10$ $cm^{-1}$ (compared to 1825 $cm^{-1}$ from matrix isolation spectroscopy[19]), $X_7$ as the $2_0^1 4_0^1$ combination band, and $X_0$ as the $5_1^1$ sequence band using $\nu_5 = 428 \pm 10$ $cm^{-1}$ for the anion. Unfortunately, the same analysis fails miserably for the $C_3D$ SEVI spectrum, as shown in the bottom half of Fig. 7.

These considerations suggest that a more sophisticated analysis of band $X$ is warranted, taking account of the large amplitude bend motion and neutral Renner-Teller effects, as mentioned above. Such an analysis is outside the scope of this paper, but we point out a few salient points of interest. In four atom molecules where Renner-Teller coupling is important,[52] degenerate vibrational levels are split into states with differing vibronic angular momentum $K = (l_4 + l_5) \pm \Lambda$, where $\Lambda = 1$ for a $\Pi$ electronic state and $l_i$ is the vibrational angular momentum in the bending mode $\nu_i$. If we label bending vibrational levels of the $\tilde{A}\,^2\Pi$ state by $|\nu_4 \nu_5\rangle$, then the $|00\rangle$ ground vibrational state has $K = 1$, while the $|1,0\rangle$ and $|0,1\rangle$ states are each split into three levels, two with $K = 0$ (the $\Sigma^\mu$ and $\Sigma^\kappa$ levels), and one with $K = 2$. In a $^2\Pi$ state, the $K \neq 0$ levels are also split by spin-orbit coupling.

Experiment and theory predict a very large Renner-Teller splitting in the $\nu_4$ mode in the $\tilde{A}\,^2\Pi$ state of $C_3H$. For example, in the theoretical treatment by Perić *et al.*,[14] the $|1,0\rangle$ level lies 589 $cm^{-1}$ above the $|00\rangle$ level in the absence of RT and spin-orbit coupling. Inclusion of these effects splits the $|00\rangle$ level into a $^2\Pi_{1/2,3/2}$ spin-orbit doublet spaced by 14 $cm^{-1}$ and brings the $\Sigma^\mu$ component of the $|1,0\rangle$ level to within only 27 $cm^{-1}$ of the $^2\Pi_{1/2}$ level, close to the experimental result obtained by analysis of the microwave spectrum.[22] As pointed out by Kanada *et al.*,[24] this very small splitting is characteristic of large amplitude bending motion in a quasilinear molecule for which the distinction between vibrational and rotational angular momenta around the symmetry axis becomes ambiguous.

We now consider photodetachment from the ground vibrational state of $l$-$C_3H^-$. Our B3LYP calculations indicate that this species is a near-prolate top, so that the rotational quantum number $K'$ about the symmetry axis (approximated by the nearly linear C–C–C skeleton) is a nearly good quantum number, so we can use some of the ideas developed to simulate the photoelectron spectrum of $HCCO^-$ where, like here, there is large amplitude bending motion in both the anion and neutral.[13] Photodetachment of the $K' = 0$ level can only access $K = 1$ levels of the $\tilde{A}\,^2\Pi$ state with vibrational angular momentum $l = l_4 + l_5 = 0$, otherwise the overlap integral between the initial and final states over the azimuthal angles describing vibration and rotation about the symmetry axis will be zero. Similarly, the $K' = 1$ rotationally excited level can only access neutral levels with $l = 1$, i.e., levels with $K = 0$ and 2. These considerations suggest an alternate explanation for peaks $X_0$ and $X_1$ in the SEVI spectra of $C_3H^-$ and $C_3D^-$, namely, that peak $X_1$ is the $K = 1 \leftarrow K' = 0$ transition to the $|00\rangle$ neutral state, while peak $X_0$ is the $K = 0 \leftarrow K' = 1$

transition to the $\Sigma^{\mu}$ component of the $|1,0\rangle$ neutral level, i.e., a transition originating from a rotationally excited level of the anion.

This assignment is consistent with the relative peak spacings and intensities of $X_0$ and $X_1$ for the two isotopologues, since, compared to $C_3H^-$, the spacing between the $K'=0$ and 1 levels in $C_3D^-$ is smaller and the population of the $K'=1$ level is higher. The assignment requires an effective rotational constant $A$ of about 70 $cm^{-1}$ for the anion, a large but perhaps not unreasonable value given the low barrier to linearity, and the large amplitude of the bending motion expected even in its ground vibrational state. The B3LYP calculation predicts a value of 52 $cm^{-1}$, which can be considered a lower bound owing to the structural rigidity inherent in the calculation. In any case, a complete assignment of band $X$ including transitions to higher vibrational levels will have to await a more sophisticated theoretical treatment.

The FC simulation of band $C(\tilde{a}\,^4\Sigma^- \leftarrow \tilde{a}\,^3A'')$ is shown overlaid on the 355 nm $C_3H^-$ spectrum in the inset of the top panel in Fig. 1. Peak $C_0$ is assigned as the band origin with and excitation energy of $1.326\pm0.018$ eV from the $^2\Pi$ state. The main progression in band $C$ is calculated to arise from activity in the $\nu_4$ HCC bend due to the large change in HCC bond angle between the $\tilde{a}\,^3A''$ and $\tilde{a}\,^4\Sigma^-$ states ($\sim 36°$, B3LYP). The HCC bend frequency was lowered from the calculated value of 263 $cm^{-1}$ to match the 250 $cm^{-1}$ spacing between $C_0$ and $C_1$. The $C_0$-$C_2$ peak spacing (411 $cm^{-1}$) reflects the value used for the $\nu_5$ CCC bend simulated frequency, which is close to the B3LYP value of 463 $cm^{-1}$. These are the only two frequencies used in the simulation since the 355 nm spectrum cuts off after $C_0$ at approximately 1185 $cm^{-1}$. The $\nu_3$ CCC symmetric stretching mode is calculated to be approximately 100 $cm^{-1}$ higher than the cutoff. In addition to adjusting the frequencies, the normal coordinate displacements of the HCC and CCC bending mode were also adjusted significantly from their calculated values. The simulation represents the best fit obtained within the harmonic FC approximation. Only the intensities of $C_1$ and $C_2$ are accurately reproduced owing to their adjustability via the corresponding normal coordinate displacements. Although the intensities of the latter peaks are significantly lacking in the simulation, peak assignments for $C_3$–$C_5$ can still be made on the basis of simulated frequencies, as shown in Table I. As discussed above, we expect only limited success for harmonic FC analysis of this band, so the relatively poor agreement between simulated and experimental intensities is not surprising.

## V. CONCLUSIONS

We have investigated photodetachment from two isomers of $C_3H^-$, $c$-$C_3H^-$, and $l$-$C_3H^-$, to the corresponding neutral isomers using TOF photoelectron spectroscopy and slow electron velocity-map imaging (SEVI). Several vibrationally resolved bands involving transitions to the ground and low-lying excited states of neutral $C_3H$ were observed. Transitions originating from $c$-$C_3H^-$ and $l$-$C_3H^-$ could be distinguished based on the photoelectron angular distributions and whether a particular band was more intense when propyne or acetylene was used as the anion precursor. More detailed assignments were based on comparison with electronic structure calculations and Franck-Condon simulations.

Our experiments represent the first definitive observation and characterization of $c$-$C_3H^-$ as well as several of the low-lying electronic states of both neutral isomers. Using previously calculated neutral energetics,[16] which place neutral $c$-$C_3H$ 74 meV below $l$-$C_3H$, our results show that $c$-$C_3H^-$ is the more stable anion isomer and that it lies 229 meV below $l$-$C_3H^-$. We thus obtain the electron affinities of $C_3H$ and $C_3D$ from the vibrational origin of the $\tilde{X}\,^2B_2 \leftarrow \tilde{X}\,^1A_1$ band within the cyclic manifold.

The extensive vibrational structure seen in the $\tilde{X}\,^2B_2 \leftarrow \tilde{X}\,^1A_1$ band was readily assigned by Franck-Condon simulations, with the exception of the nominally forbidden $4_0^1$ transition which becomes allowed via pseudo-Jahn-Teller coupling to the nearby $\tilde{B}\,^2A_1$ state of $c$-$C_3H$. While the TOF photoelectron spectrum of the $\tilde{A}\,^2\Pi \leftarrow \tilde{a}\,^3A''$ band between $l$-$C_3H$ and $l$-$C_3H^-$ revealed only a single feature, the higher resolution SEVI spectrum showed considerable well-resolved underlying structure. Analysis of this band was problematic, however, as it involves a transition between an anion state with large amplitude, highly anharmonic bending motion, and a neutral state with strong Renner-Teller coupling. FC analysis was also used to assign vibrational features in the $\tilde{B}\,^2A_1 \leftarrow \tilde{X}\,^1A_1$ and $\tilde{a}\,^4\Sigma^- \leftarrow \tilde{a}\,^3A''$ bands within the cyclic and linear manifolds, respectively, although effects associated with anharmonic bending also complicated analysis of the intensities in the latter band.

*Note added in proof.* A recent paper by Halvick [P. Halvick, Chem. Phys. **340**, 79 (2007)] used the multiconfigurational self-consistent-field method to study the symmetry breaking problem in the $C_3H$ radical and confirmed that the neutral ground state has $C_{2v}$ symmetry.

## ACKNOWLEDGMENTS

This research is supported by the National Science Foundation under Grant No. DMR-0139064. S.M.S. thanks Professor Kent Ervin for useful discussions. Etienne Garand thanks the Natural Science and Engineering Research Council for a post-graduate scholarship.

[1] R. I. Kaiser, C. Ochsenfeld, M. HeadGordon, Y. T. Lee, and A. G. Suits, Science **274**, 1508 (1996).
[2] D. C. Clary, E. Buonomo, I. R. Sims, I. W. M. Smith, W. D. Geppert, C. Naulin, M. Costes, L. Cartechini, and P. Casavecchia, J. Phys. Chem. A **106**, 5541 (2002).
[3] C. A. Gottlieb, J. M. Vrtilek, E. W. Gottlieb, P. Thaddeus, and A. Hjalmarson, Astrophys. J. **294**, L55 (1985).
[4] P. Thaddeus, C. A. Gottlieb, A. Hjalmarson, L. E. B. Johansson, W. M. Irvine, P. Friberg, and R. A. Linke, Astrophys. J. **294**, L49 (1985).
[5] S. Yamamoto, S. Saito, M. Ohishi, H. Suzuki, S. Ishikawa, N. Kaifu, and A. Murakami, Astrophys. J. **322**, L55 (1987).
[6] J. Cernicharo and M. Guelin, Astron. Astrophys. **309**, L27 (1996).
[7] M. Guelin, J. Cernicharo, M. J. Travers, M. C. McCarthy, C. A. Gottlieb, P. Thaddeus, M. Ohishi, and S. Saito, Astron. Astrophys. **317**, L1 (1997).
[8] H. Suzuki, M. Ohishi, N. Kaifu, S. Ishikawa, T. Kasuga, S. Saito, and K. Kawaguchi, Publ. Astron. Soc. Jpn. **38**, 911 (1986).
[9] S. Saito, K. Kawaguchi, H. Suzuki, M. Ohishi, N. Kaifu, and S. Ishikawa, Publ. Astron. Soc. Jpn. **39**, 193 (1987).

[10] R. I. Kaiser, C. Ochsenfeld, M. HeadGordon, Y. T. Lee, and A. G. Suits, J. Chem. Phys. **106**, 1729 (1997).
[11] K. Aoki, S. Ikuta, and A. Murakami, J. Mol. Struct.: THEOCHEM **365**, 103 (1996).
[12] J. F. Stanton, Chem. Phys. Lett. **237**, 20 (1995).
[13] B. Schäfer-Bung, B. Engels, T. R. Taylor, D. M. Neumark, P. Botschwina, and M. Poric, J. Chem. Phys. **115**, 1777 (2001).
[14] M. Perić, M. Mladenović, K. Tomić, and C. M. Marian, J. Chem. Phys. **118**, 4444 (2003).
[15] J. Takahashi and K. Yamashita, J. Chem. Phys. **104**, 6613 (1996).
[16] C. Ochsenfeld, R. I. Kaiser, Y. T. Lee, A. G. Suits, and M. HeadGordon, J. Chem. Phys. **106**, 4141 (1997).
[17] Y. M. Wang, B. J. Braams, and J. M. Bowman, J. Chem. Phys. **111**, 4056 (2007).
[18] J. C. Sancho-García and A. J. Pérez-Jiménez, J. Phys. B **35**, 3689 (2002).
[19] Q. Jiang, C. M. L. Rittby, and W. R. M. Graham, J. Chem. Phys. **99**, 3194 (1993).
[20] H. Ding, T. Pino, F. Guthe, and J. P. Maier, J. Chem. Phys. **115**, 6913 (2001).
[21] S. Yamamoto and S. Saito, Astrophys. J. **363**, L13 (1990).
[22] S. Yamamoto, S. Saito, H. Suzuki, S. Deguchi, N. Kaifu, S. I. Ishikawa, and M. Ohishi, Astrophys. J. **348**, 363 (1990).
[23] S. Yamamoto and S. Saito, J. Chem. Phys. **101**, 5484 (1994).
[24] M. Kanada, S. Yamamoto, S. Saito, and Y. Osamura, J. Chem. Phys. **104**, 2192 (1996).
[25] K. Aoki, K. Hashimoto, S. Ikuta, and O. Nomura, Chem. Phys. Lett. **242**, 527 (1995).
[26] S. Ikuta, J. Chem. Phys. **106**, 4536 (1997).
[27] N. M. Lakin, M. Hochlaf, G. Chambaud, and P. Rosmus, J. Chem. Phys. **115**, 3664 (2001).
[28] D. E. Woon, Chem. Phys. Lett. **244**, 45 (1995).
[29] M. Pachkov, T. Pino, M. Tulej, and J. P. Maier, Mol. Phys. **99**, 1397 (2001).
[30] T. Pino, M. Pachkov, M. Tulej, R. Xu, M. Jungen, and J. P. Maier, Mol. Phys. **102**, 1881 (2004).
[31] J. M. Oakes and G. B. Ellison, Tetrahedron **42**, 6263 (1986).
[32] M. Kohno, H. Shiromaru, and Y. Achiba, Atomic Collision Res. Jap. **20**, 115 (1994).
[33] C. Xu, G. R. Burton, T. R. Taylor, and D. M. Neumark, J. Chem. Phys. **107**, 3248 (1997).
[34] R. B. Metz, A. Weaver, S. E. Bradforth, T. N. Kitsopoulos, and D. M. Neumark, J. Phys. Chem. **94**, 1377 (1990).
[35] A. Osterwalder, M. J. Nee, J. Zhou, and D. M. Neumark, J. Chem. Phys. **121**, 6317 (2004).
[36] G. Markovich, R. Giniger, M. Levin, and O. Cheshnovsky, J. Chem. Phys. **95**, 9416 (1991).
[37] J. Cooper and R. N. Zare, J. Chem. Phys. **48**, 942 (1968).
[38] U. Even, J. Jortner, D. Noy, N. Lavie, and C. Cossart-Magos, J. Chem. Phys. **112**, 8068 (2000).
[39] E. P. Wigner, Phys. Rev. **73**, 1002 (1948).
[40] C. T. Lee, W. T. Yang, and R. G. Parr, Phys. Rev. B **37**, 785 (1988).
[41] A. D. Becke, J. Chem. Phys. **98**, 1372 (1993).
[42] T. H. Dunning, J. Chem. Phys. **90**, 1007 (1989).
[43] M. J. Frisch, G. W. Trucks, H. B. Schlegel, G. E. Scuseria, M. A. Robb, J. R. Cheeseman, J. Montgomery, J. A. T. Vreven, K. N. Kudin, J. C. Burant, J. M. Millam, S. S. Iyengar, J. Tomasi, V. Barone, B. Mennucci, M. Cossi, G. Scalmani, N. Rega, G. A. Petersson, H. Nakatsuji, M. Hada, M. Ehara, K. Toyota, R. Fukuda, J. Hasegawa, M. Ishida, T. Nakajima, Y. Honda, O. Kitao, H. Nakai, M. Klene, X. Li, J. E. Knox, H. P. Hratchian, J. B. Cross, C. Adamo, J. Jaramillo, R. Gomperts, R. E. Stratmann, O. Yazyev, A. J. Austin, R. Cammi, C. Pomelli, J. W. Ochterski, P. Y. Ayala, K. Morokuma, G. A. Voth, P. Salvador, J. J. Dannenberg, V. G. Zakrzewski, S. Dapprich, A. D. Daniels, M. C. Strain, O. Farkas, D. K. Malick, A. D. Rabuck, K. Raghavachari, J. B. Foresman, J. V. Ortiz, Q. Cui, A. G. Baboul, S. Clifford, J. Cioslowski, B. B. Stefanov, G. Liu, A. Liashenko, P. Piskorz, I. Komaromi, R. L. Martin, D. J. Fox, T. Keith, M. A. Al-Laham, C. Y. Peng, A. Nanayakkara, M. Challacombe, P. M. W. Gill, B. Johnson, W. Chen, M. W. Wong, C. Gonzalez, and J. A. Pople, GAUSSIAN 03, Revision C.02 (Gaussian, Inc., Wallingford, CT, 2004).
[44] M. Perić, M. Mladenović, and B. Engels, Chem. Phys. Lett. **393**, 552 (2004).
[45] F. Duschinsky, Acta Physicochim. URSS **7**, 551 (1937).
[46] K. M. Ervin, T. M. Ramond, G. E. Davico, R. L. Schwartz, S. M. Casey, and W. C. Lineberger, J. Phys. Chem. A **105**, 10822 (2001).
[47] K. M. Ervin, FORTRAN PESCAL (2001).
[48] K. M. Ervin, J. Ho, and W. C. Lineberger, J. Chem. Phys. **91**, 5974 (1989).
[49] T. R. Taylor, C. S. Xu, and D. M. Neumark, J. Chem. Phys. **108**, 10018 (1998).
[50] K. R. Asmis, T. R. Taylor, and D. M. Neumark, J. Chem. Phys. **111**, 8838 (1999).
[51] S. M. Sheehan, G. Meloni, B. F. Parsons, N. Wehres, and D. M. Neumark, J. Chem. Phys. **124**, 064303 (2006).
[52] M. Perić, B. Ostojić, and J. Radić-Perić, Phys. Rep., Phys. Lett. **290**, 283 (1997).